Supporting Information for

The Evolving Paradigm of the Subauroral Geospace

Evgeny V. Mishin

Air Force Research Laboratory, Space Vehicles Directorate, Albuquerque, NM, USA

Supporting Information aims to introduce the essential elements and processes in the inner magnetosphere and magnetotail characteristic of the magnetospheric substorm to give the necessary background for readers unfamiliar with the problem.

1 Motion of Test Particles in the Inner Magnetosphere

It is instructive to outline motion of test particles in the plasma sheet under the action of the large-scale corotation, E_{cor}, and superposed dawn-to-dusk, E_{dd}, electric fields (e.g., Ejiri et al., 1980). The guiding centers are subject to $\mathbf{E}\times\mathbf{B}$ and magnetic-gradient drifts. In an inertial coordinate system with the magnetic field **B** as a rotating dipole, the gradient-curvature drift in the equatorial plane is (e.g., Ejiri et al., 1980)

$$\boldsymbol{V}_{gc} = -\boldsymbol{e}_{\phi} L^2(\varepsilon_{\perp} + 2\varepsilon_{\|})/qB_0R_E \approx -3(e/q)(L/5)^2(\varepsilon_{\mathrm{keV}}/20)\boldsymbol{e}_{\phi}\ [\text{h-LT/h}] \qquad \text{(S1)}$$

Here $q = \pm e$ is the ion/electron charge, $\mathbf{e}_{\phi}$ is a unit vector positive eastward, $\varepsilon_{\perp,\|}$ is the transverse/parallel energy, L is the McIlwain L-shell value, $B_0 \approx 0.3$ G, and R_E is the Earth radius. Note, the radius of the field line curvature in a dipole field is $\mathbf{R}_c = LR_E\mathbf{e}_r$.

The corotation velocity amounts to $\mathbf{V}_{cor} = \mathbf{\Omega}_E \times \mathbf{e}_r = \mathbf{e}_{\phi}\Omega_E r\cos\theta$, where $\Omega_E = 7.3\ 10^{-5}\ \mathrm{s}^{-1}$ is the angular speed of the Earth's rotation to the east. The corotation electric potential is

$$\Phi_{cor} = -\Omega_E R_E^3 B_0 / r = -C_{cor} R_E / r,\ \text{with}\ C_{cor} = 92.4\ \ [\text{kV}]$$

($C_{cor}/R_E \approx 15$ mV/m). For ions to drift to the west, V_{gc} (1) must overcome corotation. That is, the ion kinetic energy, ε, at the magnetic equator should exceed $\varepsilon_{\mathrm{cor}} \approx eB_0\Omega_E R_E^2 L^{-1} \sim 20L^{-1}$ keV. It takes a few hours for ~20 keV ions to propagate from midnight to dusk at $L \sim 4$-6. Note that the test-particle approach predicts the "nose" distribution of westward-drifting energetic ions and eastward-drifting electrons (e.g., Ejiri et al., 1980).

For ballpark estimates of the convection electric field one can use the Volland-Stern model (Volland, 1973; Stern, 1975) with the shielded potential in the magnetic equatorial plane

$$\Phi_{VS} = -Ar^{\gamma}\sin\varphi \qquad \text{(S2)}$$

Here γ is the shielding constant, $\varphi = \pi$ (MLT/12 – 1) is azimuthal angle; R is geocentric radial distance, and the coefficient $A = 0.045A_0\ [\mathrm{kV}/R_E^2]$ with $A_0 \sim 1$ depending on the level of geomagnetic activity. The total (Volland-Stern + corotation) potential and electric field are ($\gamma = 2$)

$$\Phi_{tot} = \Phi_{VS} - C_{cor} R_E / r$$
$$\mathbf{E}_{tot} = -\nabla \Phi_{tot} = -\mathbf{e}_r C_{cor} R_E / r^2 + A(2\mathbf{e}_r \sin\varphi + \mathbf{e}_\phi \cos\varphi) r \tag{S3}$$

1.1 Alfvén Layer

The potential (eq. S3) produces two classes of the equipotentials that coincide with the drift trajectories of $\mathbf{E}\times\mathbf{B}$-drifting cold particles. Near the Earth, potential lines are continuous or closed around the Earth. At larger distances, they extend from the geomagnetic tail, towards and around the closed-contour region and out to the dayside magnetopause. The separatrix between open and closed drift trajectories is termed the *Alfvén layer*. For cold plasmaspheric particles, it coincides with the stagnation curve, $r = R_s(\varphi)$, where E_{tot} (eq. S3) is zero. As the cold population is preserved at $r \le R_s(\varphi)$ but lost on open trajectories, $R_s(\varphi)$ designates the (cold) plasmasphere's boundary–the *plasmapause*. Similarly, the nightside Alfvén layer of ≥1 keV ("*hot*") electrons is the PS inner boundary, which maps down to the auroral boundary. The contribution of the gradient-curvature drift (eq. S1) makes the Alfvén layer location of hot particles depend on the particle kinetic energy, with the more energetic particles farther from Earth relative to their less-energetic counterparts. This creates the "dispersive" PS/auroral boundary, $r = R_A(\varphi, \varepsilon)$, on a large scale determined by the field line curvature.

1.2 Large-Scale FACs

In a quasi-stationary state, large-scale field-aligned currents (FACs) are described by the Vasyliunas (1970) formula

$$j_{\parallel}^{(M)} = \mathbf{b}_M \cdot \left[\nabla_\perp \tilde{V} \times \nabla_\perp P \right]_M \tag{S4}$$

Here $\mathbf{b} = \mathbf{B}/B$, $\tilde{V} = \int_0^s B^{-1} ds'$ is the flux tube volume of unit magnetic flux, "M" stands for "equatorial Magnetosphere," and the integral is taken along **B** from the equatorial plane point where $j_{\parallel}^{(M)} = 0$ to the ionospheric foot point. That is, FACs appear when the isocontours of $\tilde{V}$ and pressure, P_M, misalign. In the ring current (RC) region, $\tilde{V}$ depends primarily on the radial distance. Thus, the main contribution to duskside Region 2 (R2) FAC comes from the azimuthal gradient, $\partial P_{RC}/\partial\varphi$, which is built up in disturbed conditions by westward-drifting energetic ions (eq. S1).

2 Magnetotail Mesoscale Plasma Flows and Dipolarization Fronts

Intermittent fast Mesoscale (hot, ≥1 keV) Plasma Flows (MPFs), commonly referred to as bursty bulk flows or BBFs (Angelopoulos et al., 1994), are ubiquitous in the near-Earth tail, $10 < r/R_E < 30$, particularly in the pre-midnight sector (e.g., Sitnov et al., 2019 and references therein). A typical BBF is a narrow, enhanced flow channel, dawn-dusk extent of 1-3 R_E and likely localized in Z direction within 1–2 R_E, lasting from a few to 10-20 minutes and comprising smaller-scale flow bursts at V_X ~400-1000 km/s that persist for 10s-100 seconds. The flow peak velocity decreases significantly at $R < 12R_E$, indicating that BBFs tend to stop (brake) in the inner magnetosphere (Shiokawa et al., 1997). The ionospheric signatures of earthward mesoscale flow bursts are longitudinally narrow, roughly north-south oriented auroral forms that first appear at the poleward boundary of the auroral oval and expand largely equatorward. Such arcs -- the footprint of earthward propagating MPFs -- are referred to as auroral streamers (e.g., Sergeev et al., 2004).

Embedded in MPFs are localized "*dipolarization*" regions, i.e., a passing transition from the stretched tail to a more dipole-like configuration. That is, the vertical (northward) magnetic component, B_Z, in a few seconds increases at the front, thus making a region of an enhanced magnetic pressure termed the "dipolarizing flux bundle" or DFB (e.g., Liu et al., 2014). It is separated from the ambient plasma by a sharp "dipolarization front" (DF) of the thickness, $\delta X_f \sim$ 500-1000 km, comparable to the ion gyroradius in the downstream flow. The magnetic variation at the boundary of tenuous DFB plasma and denser downstream plasma creates the Hall current, $J_Y = -\partial B_Z/\mu_0\partial X \leq 40$ nA/m^2, greater than the ambient tail current by 5-10 times.

The polarization electric field in DFs, $\mathbf{E}_X = (ne)^{-1}\mathbf{J}_Y \times \mathbf{B}_Z$ is typically ~5-10 mV/m; occasionally up to 20 -30 mV/m (Runov et al., 2011; Fu et al., 2012). It creates a few kV voltage, which may reflect and accelerate the surrounding plasma particles. In the upstream region, however, the characteristic gradient scale is greater than the ion gyroradius and the convection term becomes dominant. The Hall current and the cross-tail electric field, $E_Y \leq 10$ mV/m, yields Joule heating at the front, $Q_{DF} = \mathbf{J}_Y \cdot \mathbf{E}_Y$, up to 10^{-10} W/m^3. This makes DFs important dissipation sites in the substorm magnetotail (Angelopoulos et al. 2013). The electrons–the DF current carriers– are heated at the front, most likely, via resonant interactions with broadband intense waves associated with DFs (e.g., Divin et al., 2015) and excited by a plasma instability driven by the cross-tail electron drift in the front.

2.1 MHD Approach: Plasma "Bubbles"

The ideal-MHD approach considers BBFs with depleted density as flux tubes with reduced entropy, $S = P\tilde{V}^{5/3}$ ($\tilde{V}$ is the flux tube volume), or "bubbles", as compared to the surroundings (e.g., Wolf et al., 2009; Birn et al., 2011). Such bubbles, as an air bubble in water, can slip earthward with respect to their neighbors due to a magnetic buoyancy force caused by the interchange instability. Namely, the gradient-curvature drift, $\mathbf{V}_{gc}$ (eq. S1) in a curved magnetic field plays a role of the gravitational drift with the effective "gravitational acceleration" along the radius of the field line curvature, $m_i \boldsymbol{g}_i^{(gc)} \propto T_i \boldsymbol{R}_c \times \boldsymbol{B}$. The curvature radius in a dipole field, $\mathbf{R}_c = LR_E\mathbf{e}_r$, is inapplicable for the DF configuration. More appropriate is a Harris-like geometry, with the neutral sheet at z = 0 and the half thickness of Δz_l:

$$\mathbf{B} = (B_X(z), 0, B_Z = \text{const}) \text{ with } B_X(z) = B_{lobe}\tanh(z/\Delta z_l) \qquad \text{(S5)}$$

At $B_Z \gg B_X$, one gets $\boldsymbol{R}_c \approx -\boldsymbol{e}_X \Delta z_l B_Z/B_{lobe}$. The instability condition, $\boldsymbol{g}_i^{(gc)} \cdot \nabla n < 0$, is satisfied for the DF earthward density gradient ($l_n \sim \delta X_f$). Thus, the tenuous ("light") plasma inside the DF moves opposite to $\mathbf{R}_c$, that is, earthward. A bubble is supposed to stop in the inner magnetosphere when the bubble's entropy levels with the surrounding PS plasma (e.g., Dubyagin et al., 2011); though, no consensus has been reached on the actual cause so far. Mishin and Streltsov (2021) noticed that the ambient plasma of the density $n_p \gg n_f$ can effectively slow down interchange instability-driven bubbles because the instability growth rate reduces as $(n_f/n_p)^{1/2} \ll 1$. In addition to the ambient plasma effect, enhanced plasma turbulence at the front can efficiently demagnetize the MPF's ions (see eq. (S10)) and entirely suppress the instability development and bubble's motion.

There exist also a two-fluid approach to the dynamics of bounded plasma jets (plasma beams) in transverse magnetic fields known as the self-polarization penetration through magnetic barriers.

2.2 Self-Polarization Penetration across Magnetic Barriers

Since Bostick's (1956) pioneering work till recent Gavrilov's (2021) experiments, numerous investigations explored in what way a plasma beam of the density/speed, n_b/V_b, can move across the magnetic field when the ram pressure, $P_b = n_b m_i V_b^2/2$, is smaller than $P_\perp = B_\perp^2/2\mu_0$ (the magnetic pressure) or $\beta_b = \mu_0 n_b m_i V_b^2/B_\perp^2 \ll 1$. Schmidt (1960) was the first to recognize the key role of polarization charges at the flanks of a low-β beam. The polarization electric field, $\mathbf{E}_{pol}$, arises from the opposite deflection of the beam ions and electrons because of the Lorentz force, and allows the beam to propagate at essentially the initial speed, v_b. This motion is appropriately termed the "self-polarization penetration" or simply the "self-polarization". The state of the art of this problem is described in (Brenning et al., 2005; Hurtig et al., 2005; Gunell et al., 2008; Mishin, 2013; Voitcu and Echim, 2016; Mishin and Streltsov, 2021, Chapter 3.1).

In an "ideal" magnetic barrier configuration, the barrier (downstream) magnetic field is purely transverse, $\mathbf{B}_d = \mathbf{B}_\perp$, and the upstream field is absent, $B_u = 0$. Let a slab-shaped beam of the transverse size, $a_\perp$, is incident at a velocity $\boldsymbol{V}_b = V_0 e_X$ upon a magnetic barrier, $\mathbf{B}_Z = B_d(X)\mathbf{e}_Z$. As ions move ahead of electrons, a "primary," upstream-directed polarization field, $\delta E_X \sim -n_b e \delta \boldsymbol{X}/\epsilon_0$, appears at the forefront. It drives the $\delta\mathbf{E}_X \times \mathbf{B}_d$ electron drift, creating a "secondary" polarization field, $E_{pol} \to V_0 B_d \times \boldsymbol{e}_X$, such that the $\mathbf{E}_{pol} \times \mathbf{B}_d$ -drifting electrons catch up with the ions, and the beam moves further. This essentially stepwise process implies that the beam ram pressure, P_b, greatly exceeds the energy density of the polarization field, $P_E \approx \epsilon_0 (V_b B_d)^2/2$, or

$$P_b/P_E = n_b m_i/\epsilon_0 B_d^2 = n_b m_i c^2/\mu_0 B_d^2 = c^2/v_A^2 = \epsilon_\perp - 1 \approx \epsilon_\perp \gg 1 \qquad \text{(S.6)}$$

Here $\epsilon_\perp$ is the transverse (Alfvén wave) dielectric permittivity and $v_A = \sqrt{B_d^2/\mu_0 m_i n_b}$ is the Alfvén speed in the beam. This condition ensures that $a_\perp$ is much wider than the polarization charge layer, $\delta Y_c = \delta_c \sim a_\perp/\epsilon_\perp$. Otherwise, a significant fraction of the beam's population in the layer would be lost, as revealed in experiments (e.g., Wessel et al., 1990) and simulations (e.g., Galvez and Borovsky, 1991). A stricter criterion for $\epsilon_\perp$ follows from the condition that the moving ahead ions are not stopped by the emerging voltage, $\Delta\Phi \sim \delta E_X \delta X$, before the polarization charge set in. This condition yields $\epsilon_\perp \gg \sqrt{m_i/m_e}$ (Peter and Rostoker, 1982). The actual "self-polarization" limit was established in the Ishizuka and Robertson (1982) experiment:

$$P_b/P_E \approx \epsilon_\perp > \epsilon_\perp^{(sp)} \approx 10\sqrt{m_i/m_e} \quad \text{or}$$
$$n_b > n_b^{(sp)} \approx 10\epsilon_0 B_d^2/\sqrt{m_e m_i} \approx (B_d[\text{nT}]/650)^2 \ \text{cm}^{-3} \qquad \text{(S7)}$$

Beams with $n_b < n_b^{(sp)}$ will stop in the transition region due to developing electrostatic oscillations (Peter and Rostoker, 1982).

2.2.1 Beam Width and Anomalous Diffusion

The beam ions slow down when they enter the high potential side (e.g., Brenning et al., 2005). To overcome the polarization field potential, their gyroradius must exceed the beam diameter, i.e., $a_\perp \le m_i V_b/2eB_d = r_b/2$. This suggests that a wide beam may split due to an interchange instability into several beams of widths ~$r_b/2$, and each of those with $\epsilon_\perp > \epsilon_\perp^{(sp)}$ will propagate independently.

If beams carry the transverse magnetic field, $B_{Zu} \neq 0$, the limiting width increases (Gunell et al., 2008)

$$a_\perp < a_{\perp m} = \frac{r_b}{2} \frac{B_d}{B_d - B_{Zu}} \tag{S8}$$

Note, there is no barrier for $\Delta B_\perp = B_d - B_{Zu} \to 0$. This implies negligible diffusive processes at the front. However, if the downstream field permeates the front faster than its motion is halted, the limit (eq. S8) is relaxed if not extinct. Let us assume beams moving across a gradually increasing transverse magnetic field with the gradient scale, $l_B = \left| d \ln(B_Z) / dX \right|^{-1} \gg \delta X_f$ (the front thickness). Then, the limit (eq. S8) relaxes to (Mishin, 2013).

$$a_{\perp m} \approx \tfrac{1}{2} l_B \begin{cases} r_b / \delta X_f, \text{ slow magnetic diffusion} \\ \alpha_m, \text{ fast magnetic diffusion} \end{cases} \tag{S9}$$

Here $1 < \alpha_m = r_b / \delta X_f \lesssim \sqrt{m_i / m_e}$. The fast penetration can result from "anomalous" magnetic diffusion due to an instability at the front mainly driven by the electron Hall current (Mishin et al., 1986; Brenning et al., 2005). Mishin et al. (1986) explained fast magnetic diffusion in an artificial plasma beam via the modified two-stream (lower hybrid) instability, which gives ν_{eff} of the order of the lower hybrid resonance, ω_{lhr}. A broadband turbulence associated with the fast diffusion in the self-polarization regime is observed in numerous experiments with high and low β_b (e.g., Wessel et al., 1990; Hurtig et al., 2005). The wave spectrum, like that in DFs, comprises multiple ion cyclotron harmonics and oblique lower hybrid waves.

Notably, the hot ions are demagnetized when their motion becomes chaotic under the action of enhanced low-frequency wave fields (Karney, 1978). For ions with $v_\perp > \omega_k / k_\perp$, the orbit chaotization condition gives the lower limit for the r.m.s. amplitude of lower hybrid waves (Mishin, 2013)

$$\frac{\delta E_{rms}[\frac{\text{mV}}{\text{m}}]}{B_z[\text{nT}]} > \frac{10^{-6}}{4} \left(\frac{\omega_k}{\omega_{ci}} \right)^{2/3} \frac{\omega_{ci}}{k_\perp} \tag{S10}$$

Here $k_\perp$ is in m^{-1}. For lower hybrid waves at $\omega_k \sim \omega_{lhr}$ and $k_\perp \sim 1/r_{ce}$, this condition becomes $\delta E_{rms}^{LH} > 10^{-3} B_z \sqrt{T_{pe}}$ mV/m, where B_z is in nT and the plasma electron temperature T_e is in eV. Taking B_z ~300 nT and $T_e \sim 0.5$ eV yields $\delta E_{rms}^{LH} > 0.2$ mV/m. For fast magnetosonic waves at $\omega_k \sim 10\omega_{ci}$ and $k_\perp \sim 1/3r_{ce}$, the chaotization condition (eq. S10) reads $\delta E_{rms}^{MS} > 0.3$ mV/m. In the region of enhanced waves the hot ions "slip" with respect to the magnetic field lines, thereby violating the frozen-in condition.

A kinetic numerical model of the dynamics of a plasma slab in a transverse magnetic field (Echim et al., 2005) confirms two-fluid results that the slab proper (core) moves with a uniform velocity, $\mathbf{V}_X = \mathbf{V}_0 = \mathbf{E}_{pol} \times \mathbf{b}/B$. In addition to the hydrodynamic solution, two asymmetric plasma "wings" are formed at the slab flanks. The plasma velocity inside the wings decreases from $\mathbf{V}_0$ to a minimum value in the center. Here, a flow reversal is found with the plasma convecting in the opposite direction to the core motion, like a vortex structure near the flanks of a plasma bubble.

So far, it was implied that the ambient plasma is absent (vacuum) or so tenuous that its effect is negligible. In general, background plasma electrons tend to neutralize (short out) the charge layers.

2.2.2 Short-Circuiting by the Ambient Plasma

If polarization shorting occurs faster than the polarization charges are created, viz. $\tau_\parallel < \tau_c \sim 1/\epsilon_\perp \omega_{ci}$, then the polarization field strongly decreases. Roughly a 50% reduction in the ion current density, compared to vacuum propagation, was measured for $n_p \sim 30 n_b$, while no propagation for $n_p \sim 10^2 n_b$ (Wessel et al., 1990). Taking the neutralization time of the order of the plasma wave period, viz., $\tau_\parallel \sim 2\pi/\omega_{pe}$, Wessel et al. (1990) arrived at the critical plasma density:

$$4\pi/\omega_{pe} < \tau_c \sim 1/\epsilon_\perp \omega_{ci} \rightarrow n_p > n_p^{(min)} \sim 4\pi^2 \mu \epsilon_\perp n_b > 4\pi^2 \mu \epsilon_{\perp p} n_b > 10 n_b \qquad \text{(S11)}$$

($\mu = \sqrt{m_e/m_i}$). Magnetized plasma electrons move mainly along the magnetic field, $\mathbf{B}_0 = \mathbf{e}_z B_0$, and carry a field-aligned current, $j_\parallel = -\nabla_\parallel \Phi / \sigma_\parallel$. Here $\sigma_\parallel = n_p e^2 / m_e \nu_e$ is the parallel conductivity, ν_e is the (effective) collision frequency of plasma electrons, and Φ is the self-consistent electric potential emerging in the surrounding plasma. Electric currents and low-frequency plasma turbulence associated with polarization shorting are documented in laboratory (e.g., Wessel et al., 1990; Zakharov et al., 2002; Hurtig et al., 2005; Gavrilov, 2021) and active space (Haerendel and Sagdeev, 1981; Gavrilov, 2021) experiments. Rozhanskii (1986) derived an approximate condition for short-circuiting of a stationary, self-polarization motion of a low-β plasma beam in a collisional ionospheric plasma

$$n_p > n_p^{(min)} \approx n_b \left(\frac{m_e \nu_e a_\perp}{4 m_i V_b} \right)^{1/2} \qquad \text{(S12)}$$

In collisionless unstable plasma, ν_e is determined by wave-particle interactions.

Let us consider whether the self-polarization scenario is applicable to MPFs. First, the self-polarization condition (eq. S7) in the dipole field yields that $n_b^{(sp)} < 0.1$ cm^{-3} at $L < L_{sp} \approx 4$. This is easily satisfied even for modest MPFs. A more serious constraint comes from the width requirement. In the equatorial plane, MPFs move across a gradually increasing vertical magnetic field with the gradient scale length, $l_B = \xi_B L R_E$. The coefficient $\xi_B < 1$ accounts for tail stretching over the dipole field. Thus, at $B_d - B_u \gg \delta B_Z$ and $\delta X_f \sim c/\omega_{pi}(n_f) \approx 220/\sqrt{n_f}$, the limit eq. (S9) reduces to

$$a_{\perp m} \approx \tfrac{1}{2} \xi_B L R_E \begin{cases} r_b / \delta X_f \sim \sqrt{\epsilon_\perp} \dfrac{V_X}{c} > \sqrt{\epsilon_\perp^{(sp)}} \dfrac{V_X}{c} \sim \dfrac{V_X\,[\mathrm{km/s}]}{400}, & \text{slow} \\ \alpha_m, & \text{fast magnetic diffusion} \end{cases} \qquad \text{(S13)}$$

3 Magnetospheric Substorms

For the sake of consistency, it is deemed essential to remind the basics of the auroral, or more generally, magnetospheric *substorm* (Akasofu, 1964; 2021; McPherron, 1972). A substorm commences (*breaks up*) when the stretched magnetotail suddenly releases (unloads) the stored energy and transforms to a less stretched or more dipolar-field shape, viz., a large-scale *dipolarization* takes place. An individual substorm comprises three main phases. The initial phase --the *growth* (or loading) phase—ends abruptly with the substorm *expansion* followed by the *recovery* phase during which a new equilibrium in the system is established. The breakup can be initiated by solar wind perturbations or occur spontaneously during a continuous energy inflow from the solar wind. The cycle of individual substorms with a typical duration of ~1 hour comprises three basic phases. The initial, growth or loading phase changes abruptly into the substorm expansion which is followed by the system recovery into a new equilibrium.

The auroral substorm starts with a sudden brightening of the prebreakup arc (PBA) near the equatorward boundary of the midnight auroral oval. Then, the arc expands azimuthally, largely westward, and in a few minutes breaks into a cluster of luminous auroral forms -- the auroral "bulge" -- created by precipitating keV electrons constituting an upward FAC. The cross-tail current from the dipolarized magnetotail is short-circuited by FACs into an auroral westward electrojet (WEJ) in the auroral bulge with the increased conductance (McPherron et al., 1973). The westernmost edge of the bulge poleward boundary expands as the westward traveling surge (WTS) with the upward FAC at its "head" (front). In the ionosphere, the front of the width ΔY_f ~100 km in longitude and a few degrees in latitude moves at a speed $V_f \geq$0.1-1 LT h/min ($\geq$3-30 km/s) and contains complex electric field and current regions on the scales of individual auroral arcs and enhanced Alfvén waves (e.g., Kepko et al., 2015).

3.1 Substorm Current Wedge

According to Boström's (1964) classification, the WTS/WEJ circuit is a Region 1 (R1) sense loop, viz., the downward FAC on the dawn/postmidnight side and the upward FAC on the dusk/premidnight side closed by the westward Hall current. This large-scale R1 loop was termed the substorm current wedge (SCW) owing to its wedge-like shape. At present, the classical SCW or SCW1L model is essentially modified by adding R2 sense currents (R2 loop) earthward of the dipolarized region (e.g., Kepko et al. 2015). The R2L currents map to lower latitudes with respect to the SCW1L and provide closure through the partial ring current. The combination of the R1 and R2 types of Boström's Type 1 system has been termed the two-loop substorm current wedge or the SCW2L (Sergeev et al., 2014).

As depicted in Figure S1, meridional/poleward Pedersen currents connect the downward R2 sense current with the upward R1 sense current in the bulge/WTS head (e.g., Gjerloev and Hoffman 2014; Akasofu, 2021; Birn and Hesse, 2013). Although meridional currents at times dominate the SCW2L circuit in the ionosphere (e.g., Kurikalova et al., 2018), the current disruption and large-scale field dipolarization are caused largely by the azimuthal R1 and R2 loops. As one expects from the Pedersen current continuity, auroral and subauroral azimuthal plasma flows connect continuously over the local auroral boundary near the bulge equatormost edge.

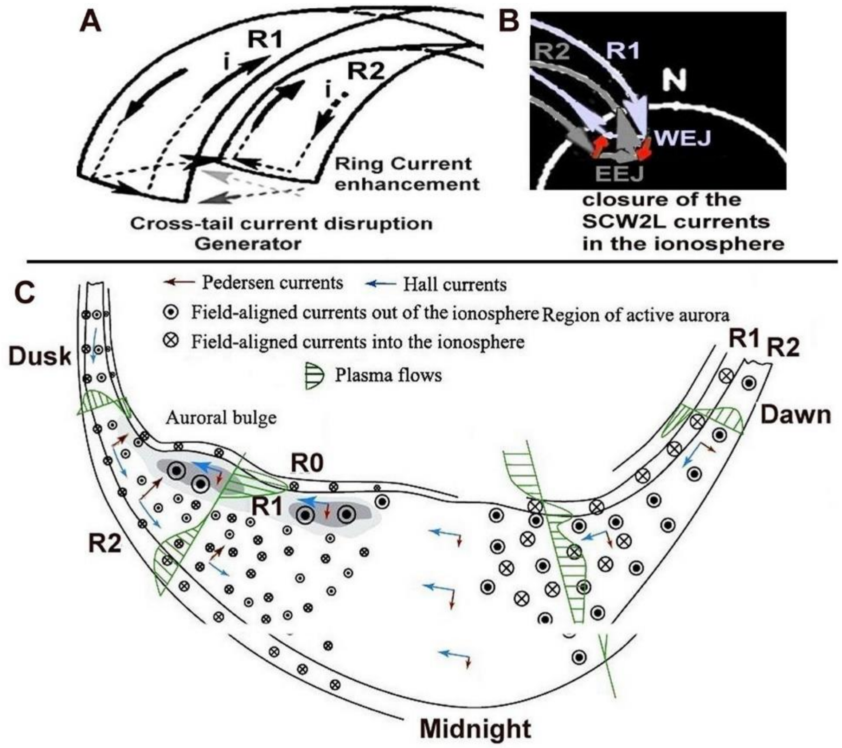

Figure S1. (A) A notional scheme of SCW2L circuit in the magnetosphere based on the Boström (1964) Type 2 current system.(B) Closure of the SCW2L circuit in the ionopshere. Red arrows indicate meridional currents. WEJ (EEJ) stands for the westward (eastward) electrojet the R1 (R2) azimuthal loops. Modified from Borovsky et al. (2020). (C) Schematic of the current and flow patterns synthesized from the Dynamics Explorer spacecraft data during the expansion phase of a magnetospheric substorm. Adapted from Kepko et al. (2015).

The bulge/WTS typically does not expand smoothly but rather stepwise, viz., in quasi-periodic bursts of activity that recur every ∼5–15 min. The steps start with an intensification of the arcs at the poleward edge followed by the equatorward ejection of streamers into the bulge (e.g., Henderson et al., 2012; Nishimura et al., 2020). Each intensification is associated with creation of new arcs poleward of the pre-existing arcs. It points to freshly arriving MPFs from the reconnection region moving tailward with the footpoint moving poleward. In general, the ionosphere adds a resistivity in the SCW2L circuit formed by the magnetospheric FACs and the ionospheric Pedersen and Hall currents. Its formation depends on the transient response of the ionosphere to magnetospheric stresses caused by the SCW development. These disturb the conjugate ionosphere via Alfvén waves carrying the current from the magnetospheric source. The closure of this current in the ionosphere provides a $\mathbf{J}\times\mathbf{B}$ force to pull the ionosphere footpoint along the magnetospheric driving.

The ionospheric response as such is determined by the Pedersen, Σ_P, and Alfvén, $\Sigma_A = 1/\mu_0 V_A$, conductances through the reflection coefficient of Alfvén waves (e.g., Glassmeier, 1984)

$$\boldsymbol{E}_r = R_A \boldsymbol{E}_i \text{ and } \delta\mathbf{B}_r = -R_A \delta\boldsymbol{B}_i \text{ with } R_A = \frac{\Sigma_A - \Sigma_P}{\Sigma_A + \Sigma_P} \approx \begin{cases} -1 \text{ at } \Sigma_P \gg \Sigma_A & \text{conductor} \\ +1 \text{ at } \Sigma_P \ll \Sigma_A & \text{insulator} \end{cases} \quad \text{(S14)}$$

Here, the subscript “i” (“r”) indicates the incident (reflected) field. The resulting FAC is

$$j_{\parallel}^{(\infty)} = j_{\parallel i}(1 - R_A)/(1 + R_A) \quad \text{(S15)}$$

As expected from general considerations, an insulator is not moved by the incident waves because $j_{\parallel}^{(\infty)}$ tends to zero and hence the ionospheric currents. At $\Sigma_P \gg \Sigma_A$, $j_{\parallel}^{(\infty)} \to \infty$ so that the ionosphere is pulled along the magnetospheric flow. In the voltage-generator magnetosphere, viz., E_M = const, precipitating electrons in the upward FAC would increase the conductivity and thus the FAC to overcome the increasing ionospheric drag. This forms a positive feedback loop, which acts to the point when the FAC or the closing currents become unstable, and the ionosphere decouples from the magnetospheric driver. This assumes the ionosphere as a resistive load, which is a reasonable assumption for the background electric field below the ionospheric feedback instability (IFI) threshold. Otherwise, the IFI makes the large-scale FACs (Alfvén waves) break into small-scale FACs/Alfvénic structures (e.g., Streltsov et al., 2012) that are easily subjected to various linear and nonlinear plasma instabilities (e.g., Mishin and Streltsov, 2021, Chapters 2.2, 2.3). At any rate, the "matching" between the conjugate magnetosphere and ionosphere requires at least several Alfvén wave bounces, typically about several minutes. No wonder that ULF, broadband, bursty geomagnetic pulsations or PiB in the Pi1 (~0.05-1 Hz) and Pi2 (~5-25 mHz) frequency ranges are used to specify the WTS initiation (e.g., Pytte et al., 1976; V. Mishin et al., 2020).

In addition, substorm injections detected by the LANL spacecraft at a geosynchronous orbit, L = 6.6, are used to mark incoming MPFs/DFs near midnight. Such "standard" (dispersionless) substorm injections have long been interpreted in terms of an electromagnetic pulse/DF propagating earthward at an average speed of ~20- 100 km/s and then expanding azimuthally (e.g., Liou et al., 2001). The front picks up magnetotail particles that are betatron-accelerated and after their release in the inner magnetosphere drift at $\boldsymbol{V}_{gc}$ (eq. S1). Ion and electron injection regions are spatially offset by ~1–2 min/h-LT according to the drift direction and expand azimuthally in both eastward and westward directions at speeds up to ~2 h-LT/min away from the onset meridian (Thomsen et al., 2001).

On a global scale, the westward electrojet transforms the pre-substorm, two-cell DP2 convection into the one-cell, or DP1 system, which makes the H magnetic component on the ground plunge down, hereby indicating the substorm onset. The auroral electrojet index (AE) -- the difference between the auroral electrojet upper (AU) and lower (AL) indices – is used as a quantitative measure of the auroral magnetic activity. The AL (AU) index specifies a minute-averaged intensity of the westward (eastward) auroral electrojet. As a rule of thumb, the transition time from the DP2 current system to DP1 and the excursion magnitude, the AE index, characterize the intensity and expansion rate of the SCW/WTS current circuit.

3.2 Substorm Breakup and Mesoscale Flows/Streamers

The buildup of the SCW-creating pressure gradient in the near tail is attributed to hot plasma jets arriving at their terminus, L_{ts} (e.g., Kepko et al., 2015; Ebihara and Tanaka, 2020). Nishimura et al. (2010) explored isolated substorms with the pre-onset auroral sequence initiated by poleward boundary intensifications followed by auroral streamers extending equatorward to the vicinity of the auroral onset facilitated by the "touch" of a prebreakup streamer. In other words, the streamer-related MPFs approaching the PS pre-onset boundary trigger the breakup. However, not every streamer "touching" the PBA initiates the onset (e.g., Henderson, 2012; 2022; Miyashita and Ieda, 2018). Sometimes, the PBA brightening ends up as a localized auroral activation without the significant poleward-westward expansion. Such events are known as pseudo-substorms or pseudobreakups.

According to Fukui et al. (2020), the substorm-related MPFs persist somewhat longer and penetrate closer to the Earth in a wider range of MLT. They are, on average, accompanied by the substantially larger dipolarization effect persisting longer and resulting in ~80% larger earthward magnetic flux transport rates, as compared to the non-substorm MPFs. Furthermore, the total pressure created by the substorm-related MPFs at $8 \le |X|/R_E \le 11$ for several minutes prior to onset was larger than that for pseudobreakups. As intuitively sounds sensible, these features suggest that, most likely, the MPFs' "strength" is the key factor. The role of earthward-propagating mesoscale flow bursts/auroral streamers in the substorm development is thoroughly examined in (e.g., Henderson, 2002; 2021; 2022; Kepko et al., 2015; Lyons and Nishimura, 2020; Nishimura et al., 2014). As shown by Henderson (2002; 2022), more typically, streamers and hence MPFs result in mesoscale auroral forms, such as torches and omega bands and then some torches can intensify and grow into onsets, substantially lagging the streamer/MPF arrival.

Wang et al. (2021) investigated by means of the RCM-UCLA code the breakup development due to the hypothetical ion demagnetization ("slippage") in the central plasmasheet. Mishin and Streltsov (2021) proposed that enhanced plasma turbulence at the MPF's front could efficiently demagnetize the ions and entirely suppress the kinetic ballooning interchange instability -- the driver of the preonset eastward-propagating ion drift waves (e.g., Sitnov et al., 2019). Still, the electron diamagnetic currents around the electron pressure peak can drive both eastward and westward propagating electron drift waves.

4 References

Akasofu, S. (1964). The development of the auroral substorm. *Planet. Space Sci.*, 12, 273-282.

Akasofu, S.-I. (2021). A review of studies of geomagnetic storms and auroral/magnetospheric substorms based on the electric current approach. *Frontiers Astr. Space Sci*., 7:604750. DOI: 10.3389/fspas.2020.604750.

Angelopoulos, V., C. Kennel, F. Coroniti, et al. (1994), Statistical characteristics of bursty bulk flow events, *J. Geophys. Res*., 99, 21,257–21,280, doi:10.1029/94JA01263.

Angelopoulos, V., A. Runov, X.-Z. Zhou, D.L. Turner, S.A. Kiehas, S.S. Li, Shinohara, I. (2013). Electromagnetic energy conversion at reconnection fronts. *Science,* 341(6153), 1478–1482. https://doi.org/10.1126/science.1236992.

Birn, J., R. Nakamura, E. Panov, and M. Hesse (2011). Bursty bulk flows and dipolarization in MHD simulations of magnetotail reconnection. *J. Geophys. Res*., 116, A01210, doi:10.1029/2010JA016083.

Birn, J., and Hesse, M. (2013). The substorm current wedge in MHD simulations. *J. Geophys. Res. Space Physics*, 118, 3364–3376, doi:10.1002/jgra.50187.

Borovsky, J., Birn, J., Echim, M., et al. (2020). Quiescent discrete auroral arcs: a review of magnetospheric generator mechanisms. *Space Sci. Rev*., 216, 1. https://doi.org/10.1007/s11214-019-0619-5, Fig. 4.

Boström, R. (1964). A model of the auroral electrojets. *J. Geophys. Res*., 69, 4983-4999. DOI: 10.1029/JZ069i023p04983.

Bostick, W. (1956). Experimental study of ionized matter projected across a magnetic field. *Phys. Rev*., 104, 292-299, doi: 10.1103/PhysRev.104.292.

Brenning, N., Hurtig, T., and Raadu, M. (2005). Conditions for plasmoid penetration across abrupt magnetic barriers. *Phys. Plasmas*, 12, 012309, 10.1063/1.1812277.

Divin, A., Y. V. Khotyaintsev, A. Vaivads, and M. André (2015). Lower hybrid drift instability at a dipolarization front. *J. Geophys.Res. Space Physics*, 120, 1124–1132, doi:10.1002/2014JA020528.

Dubyagin, S., V. Sergeev, S. Apatenkov, V. Angelopoulos, A. Runov, R. Nakamura, W. Baumjohann, J. McFadden, and D. Larson (2011). Can flow bursts penetrate into the inner magnetosphere? *Geophys. Res. Lett*., 38, L08102, doi:10.1029/2011GL047016.

Ebihara, Y. and Tanaka, T. (2020). Evolution of auroral substorm as viewed from MHD simulations: dynamics, energy transfer and energy conversion. *Rev. Mod. Plasma Phys*., 4:2. https://doi.org/10.1007/s41614-019-0037-x.

Echim, M., Lemaire, J. and Roth, M. (2005). Self-consistent solution for a collisionless plasma slab in motion across a magnetic field. *Phys. Plasmas*, 12, 072904, https://doi.org/10.1063/1.1943848.

Ejiri, M., R. Hoffman, and P. Smith (1980). Energetic particle penetrations into the inner magnetosphere. *J. Geophys. Res*., 85, 653–663.

Fu, H., Y. Khotyaintsev, A. Vaivads, M. André, and S. Huang (2012). Electric structure of dipolarization front at sub-proton scale. *Geophys. Res. Lett*., 39, L06105, doi:10.1029/2012GL051274.

Fukui, K., Miyashita, Y., Machida, S., Miyoshi, Y., Ieda, A., Nishimura, Y., and Angelopoulos, V. (2020). A statistical study of near-Earth magnetotail evolution during pseudosubstorms and substorms with THEMIS data. *J. Geophys. Res. Space Physics*, 125, e2019JA026642. https://doi.org/10.1029/2019JA026642.

Galvez, M. & Borovsky, J. (1991). The expansion of polarization charge layers into a magnetized vacuum: Theory and computer simulations. *Phys. Fluids B: Plasma Phys.*, 3, 1892-1907, https://doi.org/10.1063/1.859658.

Gavrilov, B. (2021). How do field-aligned currents influence plasma flows? Laboratory and space plasma experiments. *Adv. Space Res*., 68, 1890-1901. https://doi.org/10.1016/j.asr.2021.04.030.

Gjerloev, J., & Hoffman, R. (2014). The large-scale current system during auroral substorms. *J. Geophys. Res. Space Physics*, 119, 4591–4606, doi:10.1002/2013JA019176.

Gunell, H., T. Hurtig, H. Nilsson, M. Koepke, and N. Brenning (2008). Simulations of a plasmoid penetrating a magnetic barrier. *Plasma Phys. Control. Fusion*, 50, 074013, 10.1088/0741-3335/50/7/074013.

Haerendel, G. and Sagdeev, R. (1981). Artificial plasma jet in the ionosphere. *Adv. Space Res., 1*, 29-46.

Henderson, M., Kepko, L., Spence, H., Conners, M., Sigwarth, J., Frank, L., et al. (2002). In Winglee, R. (Ed.). The evolution of north-south aligned auroral forms into auroral torch structures: The generation of omega bands and Ps6 pulsations via flow bursts. *Sixth international conference on substorms*. University of Washington.

Henderson, M. (2012). Auroral Substorms, Poleward Boundary Activations, Auroral Streamers, Omega Bands, and Onset Precursor Activity. In: *Auroral Phenomenology and Magnetospheric Processes: Earth and Other Planets* (eds Keiling, A, Donovan, E., Bagenal, F., and Karlsson, T.). https://doi.org/10.1029/2011GM001165

Henderson, M. (2021). Generation of subauroral longitudinally extended emissions following intensifications of the poleward boundary of the substorm bulge and streamer production. *J. Geophys. Res.: Space Phys*, 126, e2020JA028556. https://doi.org/10.1029/2020JA028556.

Henderson, M. (2022). Association of Mesoscale Auroral Structures and Breakups With Energetic Particle Injections at Geosynchronous Orbit. *Front. Astron. Space Sc*i., https://doi.org/10.3389/fspas.2022.742246.

Hurtig, T., Brenning, N. and Raadu, M. (2005). The role of high frequency oscillations in the penetration of plasma clouds across magnetic boundaries. *Phys. Plasmas*, 12, 012308, 10.1063/1.1812276.

Ishizuka, H., & S. Robertson (1982). Propagation of an intense charge-neutralized ion beam transverse to a magnetic field. *Phys. Fluids*, 25, 2353.

Karney, C. (1978). Stochastic ion heating by a lower hybrid wave. *Phys. Fluids*, 21, 1584–1599.

Kepko, L., McPherron, R. L., Amm, O., Apatenkov, S., Baumjohann, W., Birn, J., et al. (2015). Substorm current wedge revisited. *Space Sci. Reviews*, 190(1-4), 1–46. https://doi.org/10.1007/s11214-014-0124-9.

Kurikalova, M., Mishin, V. M., Mishin, V. V., Lunyushkin, S., and Penskikh, Y. (2018). Relative role of the azimuthal Pedersen current component in the substorm global electric circuit. *J. Atm. Solar-Terr. Physics*, 179, 562-568, doi: 10.1016/j.jastp.2018.09.014.

Liou, K., C.-I. Meng, P. Newell, A. Lui, G. Reeves, and R. Belian, (2001). Particle injections with auroral expansions. *J. Geophys. Res*., 106, 5873–5881.

Liu, J., V. Angelopoulos, X.-Z. Zhou, & A. Runov (2014). Magnetic flux transport by dipolarizing flux bundles. *J. Geophys. Res. Space Physics*, 119, 909–926, doi:10.1002/2013JA019395.

Lyons, L. & Nishimura, Y. (2020). Substorm onset and development: The crucial role of flow channels. *J. Atm. Solar-Terr. Phys*., 211, 105474. https://doi.org/10.1016/j.jastp.2020.105474.

McPherron, R., Russell, C., and Aubry, M. (1973). Satellite studies of magnetospheric substorms on August 15, 1968: Phenomenological model for substorms. *J. Geophys. Res*., 78, 3131-3149. https://doi.org/10.1029/JA078i016p03131.

Mishin, E., Treumann, R. and Kapitanov, V. (1986). Anomalous diffusion across the magnetic field-plasma boundary: The Porcupine artificial plasma jet. *J. Geophys. Res*., 91, 10,183–10,187.

Mishin, E. (2013). Interaction of substorm injections with the subauroral geospace: 1. Multispacecraft observations of SAID, *J. Geophys. Res. Space Phys.*, 118, 5782, doi:10.1002/jgra.50548.

Mishin, V., Tsegmed, B., Klibanova, Y., Kurikalova, M. (2020). Burst geomagnetic pulsations as indicators of substorm expansion onsets during storms. *J. Geophys. Res. Space Physics*. 125, e2020JA028521. https://doi.org/10.1029/2020ja028521.

Mishin, E. and Streltsov, A. (2021). *Nonlinear Wave and Plasma Structures in the Auroral and Subauroral Geospace*. Cambridge, MA, USA: Elsevier. ISBN: 9780128207604.

Miyashita, Y. and Ieda, A. (2018). Revisiting substorm events with preonset aurora. *Ann. Geophys.*, 36, 1419e1438. https://doi.org/10.5194/angeo-36-1419-2018.

Nishimura, Y., Lyons, L., Zou, S., Angelopoulos, V., and Mende, S. (2010). Substorm triggering by new plasma intrusion: THEMIS all-sky imager observations. *J. Geophys. Res.*, 115(A7), A07223. https://doi.org/10.1029/2009JA015166.

Nishimura, Y., et al. (2014). Coordinated ionospheric observations indicating coupling between pre-onset flow bursts and waves that leads to substorm onset. *J. Geophys. Res. Space Phys.*, 119, 3333-3344. https://doi.org/10.1002/2014JA019773.

Nishimura, Y., Lyons, L., Gabrielse, C., Weygand, J., Donovan, E., Angelopoulos, V. (2020). Relative contributions of large-scale and wedgelet currents in the substorm current wedge. *Earth, Planets & Space*, 72, 106. https://doi.org/10.1186/s40623-020-01234-x.

Peter, W. and Rostoker, N. (1982). Theory of plasma injection into a magnetic field. *Phys. Fluids*, 25, 730-735.

Pytte, T., McPherron, R., Kokubun, S. (1976). The ground signatures of the expansion phase during multiple onset substorms. *Planetary and Space Science*, 24, 1115–1132.

Rozhanskii, V. (1986). Effect of background plasma on the slowing down of a plasma beam in magnetic field. *Sov. J. Plasma Phys., 12*, 170-174.

Runov, A., Angelopoulos, V., Zhou, X.-Z., Zhang, X.-J., Li, S., Plaschke, F. & Bonnell, J. (2011). A THEMIS multicase study of dipolarization fronts in the magnetotail plasma sheet. *J. Geophys. Res.*, 116, A05216, doi:10.1029/2010JA016316.

Schmidt, G. (1960). Plasma motions across magnetic fields. *Phys. Fluids*, 3, 961.

Sergeev, V., K. Liou, P. Newell, S.-I. Ohtani, M. Hairston, and F. Rich (2004). Auroral streamers: Characteristics of associated precipitation, convection, and field-aligned currents. *Ann. Geophys.*, 22, 537– 548.

Sergeev, V., Nikolaev, A., Tsyganenko, N., Angelopoulos, V., Runov, A., Singer, H., & Yang, J. (2014). Testing a two-loop pattern of the substorm current wedge (SCW2L). *J. Geophys. Res. Space Physics*, 119, 947–963, doi:10.1002/2013JA019629.

Shiokawa, K., W. Baumjohann, and G. Haerendel (1997). Braking of high-speed flows in the near-Earth tail. *Geophys. Res. Lett*., 24, 1179–1182, doi:10.1029/97GL01062.

Sitnov, M., Birn, J., Ferdousi, B., Gordeev, E., Khotyaintsev, Y., Merkin, V. et al. (2019). Explosive Magnetotail Activity. *Space Sci. Rev.*, 215. DOI:10.1007/s11214-019-0599-5.

Streltsov, A., Jia, N., Pedersen, T., Frey, H., and Donovan, E. (2012). ULF waves and discrete aurora. *J. Geophys. Res*., 117(A9), A09227. https://doi.org/10.1029/2012JA017644.

Thomsen, M., J. Birn, J. Borovsky, K. Morzinski, D. McComas, and G. Reeves, (2001). Two-satellite observations of substorm injections at geosynchronous orbit. *J. Geophys. Res*., 106, 8405– 8416.

Vasyliunas, V. (1970). “Mathematical models of magnetospheric convection and its coupling to the ionosphere.” In: *Particles and Fields in the Magnetosphere*. pg. 60. Editor McCormac, B., New York, NY, USA: Elsevier.

Voitcu, G., & M. Echim (2016). Transport and entry of plasma clouds/jets across transverse magnetic discontinuities: Three-dimensional electromagnetic particle-in-cell simulations. *J. Geophys. Res. Space Physics*, 121, 4343-4361, doi:10.1002/2015JA021973.

Wang, W., Yang, J., Nishimura, Y., Wolf, R., Toffoletto, F., Angelopoulos, V., Knudsen, D., Donovan, E., Cui, J. (2021). Effects of ion slippage in Earth’s ionosphere and the plasma sheet. *Geophys. Res. Lett*., 48. https://doi.org/10.1029/2020GL091494 e2020GL091494.

Wessel, F., Rostoker, N., Fisher, A., Rahman, H. and Song, J. (1990). Propagation of neutralized plasma beam. *Phys. Fluids B*, 2, 1467-1473.

Wolf, R. A., Y. Wan, X. Xing, J.-C. Zhang, and S. Sazykin (2009). Entropy and plasma sheet transport. *J. Geophys. Res*., 114, A00D05, doi:10.1029/2009JA014044.

Zakharov, Y., A. Eremin, A. Orishich, P. Parys, J. Wolowski, and Woryna, E. (2002). Laboratory simulations of plasma jet propagation across geomagnetic field at presence of plasma background. *Adv. Space Res*., *29*, 1351-1356.